Biogeosciences Discuss., 11, 11061–11094, 2014
www.biogeosciences-discuss.net/11/11061/2014/
doi:10.5194/bgd-11-11061-2014

Biogeosciences Discussions
Open Access

Frozen ponds: production and storage of methane during the Arctic winter in a lowland tundra landscape in northern Siberia, Lena River Delta

M. Langer[1], **S. Westermann**[2,3], **K. M. Walter Anthony**[4], **K. Wischnewski**[1], **and J. Boike**[1]

[1]Alfred-Wegener-Institut Helmholtz-Zentrum für Polar- und Meeresforschung, Periglacial Research Section, Potsdam, Germany
[2]University of Oslo, Department of Geography, Oslo, Norway
[3]Center for Permafrost (CENPERM), Department of Geosciences and Natural Resource Management, University of Copenhagen, Copenhagen, Denmark
[4]University of Alaska Fairbanks, Water and Environmental Research Center, Fairbanks, USA

Received: 9 June 2014 – Accepted: 6 July 2014 – Published: 18 July 2014

Correspondence to: M. Langer (moritz.langer@awi.de)

Published by Copernicus Publications on behalf of the European Geosciences Union.

Abstract

Lakes and ponds play a key role in the carbon cycle of permafrost ecosystems, where they are considered to be hotspots of carbon dioxide CO_2 and methane CH_4 emission. The strength of these emissions is, however, controlled by a variety of physical and biogeochemical processes whose responses to a warming climate are complex and only poorly understood. Small waterbodies have been attracting an increasing amount of attention since recent studies demonstrated that ponds can make a significant contribution to the CO_2 and CH_4 emissions of tundra ecosystems. Waterbodies also have a marked effect on the thermal state of the surrounding permafrost; during the freezing period they prolong the period of time during which thawed soil material is available for microbial decomposition.

This study presents net CH_4 production rates during the freezing period from ponds within a typical lowland tundra landscape in northern Siberia. Rate estimations were based on CH_4 concentrations measured in surface lake ice from a variety of waterbody types. Vertical profiles along ice blocks showed an exponential increase in CH_4 concentration with depth. These CH_4 profiles were reproduced by a 1-D mass balance model and the net CH_4 production rates then inferred through inverse modeling.

Results revealed marked differences in early winter net CH_4 production among various ponds. Initial state ponds underlain by stable permafrost with little or no signs of degradation yielded low net production rates, of the order of 10^{-11} to 10^{-10} mol m^{-2} s^{-1} (0.01 to 0.14 mg_{CH_4} m^{-2} d^{-1}). In contrast, advanced state ponds exhibiting clear signs of thermal erosion yielded net CH_4 production rates of the order of 10^{-7} mol m^{-2} s^{-1} (140 mg_{CH_4} m^{-2} d^{-1}). The net production rate per square meter of advanced state ponds exceeded the maximum summer CH_4 emission rates per square meter which was measured for the average tundra landscape at the study site. Our results therefore indicate that, once a particular threshold in thermal erosion has been crossed, ponds can develop into major CH_4 sources. This implies that any future warming of the climate may result in non-linear CH_4 emission behavior in tundra ecosystems.

BGD
11, 11061–11094, 2014

1 Introduction

Up to 28 % of the land surface in permafrost landscapes has been attributed to lakes and ponds (Emmerton et al., 2007; Grosse et al., 2008; Muster et al., 2013). Several studies have emphasized that waterbodies are fundamental elements in Arctic ecosystems and exert a strong control on the Arctic heat, water, and carbon cycle (Cole et al., 2007; McGuire et al., 2009). This is especially true in permafrost landscapes, where large quantities of carbon are trapped in the frozen soils that can surround waterbodies (e.g. Hugelius et al., 2013). Any future mobilization and emission of this old carbon pool is likely to result in a positive feedback to global warming (O'Connor et al., 2010; Koven et al., 2011).

Lakes are considered to play a key role in the turnover and emission of the carbon in these permafrost reservoirs (Boike et al., 2012). Many of the studies to date have focused on the greenhouse gas emission potential of large lakes such as thermokarst lakes (Zimov et al., 1997; Walter et al., 2006; Brosius et al., 2012). However, recent studies have demonstrated that not only large Arctic lakes, but also the smaller Arctic ponds, are hotspots of CO_2 and CH_4 emission (Abnizova et al., 2012b; Laurion et al., 2010). In lowland tundra landscapes such as the Lena River Delta more than 30 % of the total inland water surface can be attributed to waterbodies with surface areas less than 1 km^2 (Muster et al., 2012). Most of the studies to date addressing greenhouse gas emissions from Arctic ponds have focused on the summer months, but a considerable carbon turnover is also possible in waterbodies during the freezing period, until the bottom sediments are completely frozen (Karlsson et al., 2013). During winter the closed ice cover inhibits the diffusion of oxygen into the water which strongly limits the oxidation of CH_4 in the water column. Several studies have demonstrated that large quantities of CH_4 are produced during the long-lasting winter period and stored in the form of bubbles within the ice cover (Walter Anthony et al., 2010; Wik et al., 2011; Boereboom et al., 2012; Walter Anthony and Anthony, 2013).

BGD
11, 11061–11094, 2014

Bubbles trapped in lake ice, resulting from a number of different processes, include ebullition bubbles, bubbles from freeze-degassing of dissolved gases, and photosynthesis bubbles. These can usually be distinguished from each other on the basis of their size, morphology, and gas content (Boereboom et al., 2012; Walter Anthony and Anthony, 2013). Ebullition bubbles originate from sediments and are usually rich in methane (40–90 vol%). Ebullition bubbles form the largest of the trapped bubbles. The diameter of individual ebullition bubbles prior to gas entrapment ranges from several millimeters to several centimeters in diameter. Individual bubbles can freeze into ice as isolated bubbles or they can merge beneath the ice before freezing occurs, to form gas pockets in ice up to several meters in diameter. Photosynthesis bubbles, in comparison to ebullition bubbles, are usually smaller than 3 mm and occur in clusters around frozen plants (Walter Anthony et al., 2010). Photosynthesis bubbles typically exhibit a frayed morphology (Walter Anthony et al., 2010; Wik et al., 2011). In contrast, tiny bubbles from freeze-degassing are formed continuously at the advancing freezing front and occur in closely spaced layers in the ice cover (Lipp et al., 1987). Due to freeze-degassing dissolved gases enrich in a very thin water layer directly at the freezing front. The saturation of dissolved gases in this thin water layer leads to bubble nucleation. The gas concentration in the growing bubbles is in equilibrium with the dissolved gases of the surrounding water (Wei et al., 2003). As soon as the bubbles are completely entrapped within the ice cover they are sealed from further gaseous exchange so that an enrichment of dissolved gases and bubble nucleation at the freezing front starts again. This results in continuous formation of freeze-out bubble layers which preserve to a certain degree information about the concentration of the dissolved gases in the water column during the time of freezing (Lipp et al., 1987; Craig et al., 1992; Killawee et al., 1998). The frequency of bubble layer formation, bubble size, and bubble shape are largely dependent on the rate of freezing (Carte, 1961; Yoshimura et al., 2008). However, a wide range of sizes of freeze-out bubbles are reported at natural freezing rates of the order of millimeters per day (Lipp et al., 1987; Yoshimura et al., 2008). Freeze-out bubbles strongly vary in shape including spherical, egg shaped, and

BGD
11, 11061–11094, 2014

tubular bubble forms (Yoshimura et al., 2008). The storage of CH_4 within the ice cover of shallow Alaskan lakes through freeze-degassing has been investigated by Phelps et al. (1998). They found that CH_4 concentrations were very low in the upper part of the ice cover, but increased rapidly with depth. They also found that the CH_4 stored in the ice cover was largely released into the atmosphere during spring melt, and that the amount of CH_4 emitted in spring equated to half of the total annual CH_4 emissions from the lake. These results served to further stress the importance of the freezing period to the carbon cycle of tundra-lake ecosystems.

In this study we present profiles derived from measurements of CH_4 concentrations in the ice cover of nine typical Arctic ponds and lakes in the Lena River Delta of north-eastern Siberia. An extensive survey of pond areas and depths has provided insights into the development stages of the various waterbodies within the area of investigation. Temperature profiles were derived from measurements in three different ponds and used to investigate their freezing behavior. A 1-D mass balance model was developed to reconstruct the storage of CH_4 within the ice cover and the CH_4 concentration profiles (derived from CH_4 concentration measurements in the ice cover) were used to infer net CH_4 production rates during the freezing period by inverse modeling.

2 Study area

The study area is located in the Lena River Delta of north-eastern Siberia, within the zone of continuous permafrost (Fig. 1). The region is characterized by an Arctic continental climate with a mean annual air temperature of about −14 °C. Winter temperatures frequently fall below −45 °C while summer temperatures can exceed 25 °C (Langer et al., 2011a; Boike et al., 2013). The cold climate results in very cold permafrost temperatures: an annual average temperature of about −9 °C has been recorded at a depth of 27 m (Boike et al., 2013). Permafrost in the Lena River Delta region is reported to extend to depths of several hundred meters (Grigoriev, 1960). The study area is located on Samoylov Island in the central part of the Lena River

BGD
11, 11061–11094, 2014

Delta (72°22′ N, 126°28′ E), an area characterized by the typical micro-relief of polygonal patterned ground formed by frost cracking and subsequent ice-wedge formation (Lachenbruch, 1962). The polygonal structures usually consist of depressed, water-saturated centers surrounded by elevated rims. These polygonal structures are present in different stages of degradation. Initial degradation often leads to the accumulation of surface water, either in the depressed polygon centers (intra-polygonal ponds) or along the troughs between the polygon rims above the ice-wedges (ice-wedge ponds) (Wetterich et al., 2008; Helbig et al., 2013; Negandhi et al., 2013). Both intra-polygonal ponds and ice-wedge ponds are usually very shallow, with water depths ranging from just a few centimeters to a few tens of centimeters. Such ponds often feature emergent vegetation, consisting mainly of hydrophilic species such as *Carex aquatilis* and *Limprichtia revolvens* (Kutzbach et al., 2007). The rims surrounding intra-polygonal ponds are mostly intact with little or no sign of degradation. However, degradation of the polygonal structures can result in ponds merging to form larger ponds that often consist of several polygons, typically showing clear signs of degradation (Helbig et al., 2013). They feature open water surfaces and lack emergent vegetation in their centers. The study area is also characterized by thermokarst (thaw) lakes, which are a result of advanced permafrost degradation associated with further thermal erosion processes (Morgenstern et al., 2013). About 50 % of the free water surface on Samoylov Island is attributed to ponds, with the remaining 50 % attributed to lakes, including both thermokarst lakes and oxbow lakes (Muster et al., 2012).

3 Methods and materials

3.1 Pond survey and classification

The distribution and sizes of waterbodies within the study area were mapped using ortho-rectified, visual and near-infrared aerial images. The study area (SA) lies on the first terrace of Samoylov Island and covers a typical wet lowland tundra landscape; it

BGD
11, 11061–11094, 2014

has a surface area of about 1.5 km^2 (Fig. 1). We used the supervised surface water classification from Muster et al. (2012) to extract a size distribution for the ponds and lakes within the area. Water depth measurements were also collected from two sub-areas (SUB I and SUB II), each of which had a surface area of about 30 000 m^2 (Fig. 1). The water depths were measured manually using a depth sounder, or using a ruler where the water levels were very low.

In this study we mainly focused on small waterbodies (ponds) smaller than 10 000 m^2. We were able to loosely distinguish three types of ponds within the study area on the basis of morphology and the degree of degradation in the surrounding polygonal tundra (Fig. 2). Initial state ponds (ISPs) are defined as ponds that occur within almost intact polygonal structures; they include both intra-polygonal ponds located in polygon centers (Fig. 2b) and ice-wedge ponds located between polygon rims (Fig. 2a). ISPs are shallow with water depths of less than 0.5 m. Their horizontal extent typically ranges from a few meters up to about 10 m, which is a typical diameter for the polygonal structures. ISPs can be interconnected with other ISPs or with larger waterbodies, but the individual polygon shape is still preserved. In contrast, advanced state ponds (ASPs) show clear signs of degradation in the surrounding polygonal tundra (Fig. 2c). The center of an ASP is much deeper due to thaw settlement in the underlying bottom sediments, so that ASPs usually have water depths greater than 0.5 m. ASPs typically range in diameter from about 10 to 50 m. Waterbodies that reach depths greater than 2 m are likely to remain unfrozen at the bottom throughout the winter, and a continuously unfrozen layer (talik) then develops in the sediments. Such waterbodies are classified as thermokarst lakes; the horizontal extent of such lakes ranges from about 50 m to several hundreds of meters. Transitional forms between the three waterbody types are also common.

BGD
11, 11061–11094, 2014

3.2 Monitoring ice cover formation

The process of ice cover formation was observed through three temperature profiles obtained from three different ponds. The temperatures were recorded using HOBO water temperature loggers (with an accuracy of ±0.5 °C) positioned along a metal wire hanging down from a small buoy anchored in the middle of each pond. The first temperature profile was from an intra-polygonal pond, based on measurements from four temperature sensors over a depth of 0.4 m. The pond was transitional between ISPs and ASPs in its level of degradation. Temperature profiles were also obtained for two typical ASPs, in each case using six temperature sensors over a depth of about 0.8 m.

The ice cover thickness in each pond was inferred using the temperature records from the individual sensors. The date on which the freezing front crossed the temperature sensor was identified by a sudden drop in temperature after a relatively long period at a constant temperature of 0 °C.

3.3 Sampling methane concentrations in lake ice

Thirteen CH_4 concentration profiles were obtained from ice blocks cut from eight ponds and one thermokarst lake during a field program in April 2011, using a chainsaw (STIHL, Germany) with a 40 cm guide bar. The ice blocks were extracted by cutting ice columns to a depth of about 35 cm, with surface dimensions of about 20 cm by 30 cm, from the ice cover. A second ice column was then cut below the hole left by the first column in order to obtain ice profiles down to a maximum depth of about 70 cm. The ice columns were cut into smaller cuboids with a base area of about 7 cm × 7 cm and a height of 10 cm. The cuboids were cleaned with a sharp and sterilized knife prior to transportation and analysis.

The ice samples were melted in 1 L plastic containers (Nalgene, USA), which were sealed with PTFE paste (Äronix, Germany). The impermeability of the containers to gas was verified by long-term testing using calibration gases prior to the analyses. The containers were flushed with nitrogen immediately after sealing in order to ensure zero

BGD
11, 11061–11094, 2014

CH_4 concentration in the head-space prior to melting. The head space volume in the containers varied between 0.3 and 0.6 L according to differences in sample volume. Possible corruption of the CH_4 concentration measurements due to microbial activity during the melt procedure was tested using acidified (10 % HCl) parallel samples, but these showed no significant differences in CH_4 concentration from the pure samples. Methane concentrations within the ice samples were determined by gas chromatography at the field station on Samoylov Island, using an Agilent GC 7890 gas chromatograph (Agilent Technologies, Germany) equipped with a Porapak Q column (1.8 m length, 2 mm ID) and a flame ionization detector (FID). Four repeat concentration measurements (five measurements in total) were performed in order to determine the measurement uncertainty.

The total CH_4 content in the ice samples was evaluated by taking into account the head space concentration, sample volume, temperature, and pressure. A correction was also made for dissolved CH_4 in the melt water using Henry's law. These procedures introduced a wide range of potential error sources into the CH_4 content measurements. Thus, the uncertainties in the total CH_4 content were determined by Monte-Carlo simulations assuming uniform uncertainty distributions for all parameters including measurement uncertainty, head space volume, sample volume, ambient temperature, and pressure (e.g. Anderson, 1976).

3.4 Modeling methane concentrations in the ice cover of ponds

The storage of methane in the ice cover of ponds was simulated using a simplified 1-D mass balance scheme, in an approach that closely resembles that used by Boereboom et al. (2012). The model was used to calculate net CH_4 production rates during the freezing process by fitting the model to the CH_4 concentration profiles obtained from the ice cover. The model simulated an ice cover growing downwards from the surface to the bottom of the pond, assuming a constant accumulation of bubbles from freeze-degassing of dissolved gases at the ice–water interface (see Appendix). Ebullition bubbles were not taken into account in the model. Despite their importance as

BGD
11, 11061–11094, 2014

an efficient mode of CH_4 emission from lakes, ebullition bubbles have small diameters relative to the lake surface area and they usually have a rare and heterogeneous distribution within a thermokarst pond, making them difficult to quantify from a limited number of small ice samples (Walter Anthony and Anthony, 2013). The heterogeneous distribution of ebullition bubbles also means that they are impossible to simulate using a simplified 1-D mass balance scheme. This limitation of the model means that the CH_4 storage, and hence the production of CH_4 in ponds, tends to be underestimated. The model results can therefore be considered to be conservative when calculating net CH_4 production rates. Since the size of bubbles from freeze-degassing depends largely on the rate of freezing (Carte, 1961), we assumed that the accumulation of freeze-out bubbles was adequately represented by a constant rate during periods of constant freezing (Yoshimura et al., 2008).

The partial pressure of CH_4 in the bubbles was assumed to be always in equilibrium with the partial pressure of CH_4 in the water column, following Henry's law. We also assumed a uniform enrichment of methane in the water column beneath the ice cover. The CH_4 enrichment (net CH_4 production) is controlled by CH_4 production and oxidation. Because of the very stable temperature conditions in shallow sediments during the freezing period from October through February we assumed constant CH_4 production and oxidation rates. The uniform distribution of dissolved CH_4 in the shrinking water column is considered a reasonable guess for the investigated very shallow waterbodies albeit concentration gradients are reported for deeper lakes. However, increased CH_4 enrichment at the bottom of the ponds would lead to underestimated net CH_4 production in the model calculations. As well as the stable temperature conditions, the model also assumed constant pressure conditions during the freezing process. Nevertheless, air pressure changes are an important factor for bubble formation in lakes and can result in layers of dense bubbles in the ice cover. Thus, the obtained ice profiles were analyzed for occurrence of bubble layers that were related to air pressure changes. The storage of bubbles in the ice cover was simulated by integrating an effective bubble cross-section (calculated as average horizontal area occupied by bubbles)

BGD
11, 11061–11094, 2014

and CH_4 concentration over the current ice cover thickness. The bubble volume stored in the ice cover was assumed to be no longer in gaseous exchange with the unfrozen waterbody. When the maximum solubility of methane in the shrinking water column was reached the model assumed that the excess methane was stored directly in the ice cover. The storage of excess CH_4 resulted in a marked increase in the methane concentration within the ice cover. The mass balance scheme results in a first order ordinary differential equation, which can be solved analytically (see Appendix). In general, the model outcome is determined by the net CH_4 production rate, the effective bubble cross-section, the ice cover growth rate, and the pond depth. The pond depth and the ice cover growth rate are measured and hence known for all sites, and the net CH_4 production rate and effective bubble cross-section can be inferred by fitting the model to measured CH_4 concentration profiles. Previous measurements within the study area have shown that the concentration of dissolved CH_4 in different ponds varies widely (between 2×10^{-9} and 7×10^{-7} mol m^{-3}) prior to the onset of freezing (Abnizova et al., 2012a). The sensitivity of the fitting procedure was therefore tested over the entire range of initial CH_4 concentrations. The model was fitted to the measured CH_4 profiles using a non-linear fitting routine provided by MATLAB. This fitting procedure included evaluation of the 95 % confidence intervals on the fitted parameters and the model output.

4 Results

4.1 Waterbody distribution and ice cover formation

Almost 14 % of the study area (SA) consists of waterbodies, of which about 60 % are less than 300 m^2 in surface area (Fig. 3a). In the sub-areas SUB I and SUB II the pond surface areas range between 0 and 300 m^2 and the maximum water depth ranges between 0 and 1.5 m. About 10 % of the tundra landscapes in SUB I and SUB II are occupied by ponds that are shallower than 0.2 m. Most of these shallow ponds fall into

BGD
11, 11061–11094, 2014

the ISP class, with little or no sign of degradation in the surrounding polygon rims. Ponds with water depths of 0.5 to 0.6 m and 0.8 to 1.0 m were found to be slightly more abundant than ponds with water depths of 0.2 to 0.4 m and 1.0 to 1.3 m (Fig. 3b). Most of the ponds with a water depth greater than 0.5 m belonged to the ASP class, which made up the largest proportion of ponds in the entire study area. Despite the wide range of water depths in the surveyed ponds the deeper ponds tended to be larger than the shallower ones which coincided with increased thaw depths beneath the deeper ponds. This tendency was especially pronounced for ponds with depths greater than 0.5 m. In contrast, ISPs with water depths of less than 0.5 m did not show any clear depth–size correlation. The size of the ISPs appeared to be mainly determined by the size of the polygonal structures.

Ice cover growth (freezing) rates were investigated in three different ponds during the winters of 2010–2011 and 2011–2012. The freezing rate detection was limited to the first part of winter since temperature profile measurements were only available to a maximum depth of about 0.8 m (see Sect. 3.2). During the winter of 2010–2011 the average growth rate of the ice cover was $0.72 \pm 0.13\,\mathrm{cm\,d^{-1}}$ (Fig. 4a). The three investigated ponds showed deviations from the linear average of up to 0.15 m, which were particularly evident from the beginning of October to the middle of November. The shallowest pond (ISP1) revealed the highest freezing rate and was completely frozen (to the bottom: a depth of about 0.4 m) by the beginning of November. The other ponds (ASP1 and ASP2) achieved a similar ice cover thickness about three weeks later. In contrast to the winter of 2010–2011, all investigated ponds showed a very consistent rate of ice cover formation during the winter of 2011–2012 (Fig. 4b), when the average growth rate of the ice cover was $1.24 \pm 0.12\,\mathrm{cm\,d^{-1}}$ with only minor deviations from the linear average (up to about 0.05 m, which is well within the assumed measurement uncertainty). Despite the linear character of the freezing process, the measurements showed some temporal variations in the freezing rate. During both winter periods pond ISP1 showed a very linear freezing behavior but, in contrast, the deeper ponds showed a lower rate of freezing at the beginning of the freezing period, a slightly increased

BGD
11, 11061–11094, 2014

rate in the middle of the period, and a lower rate again when the ice cover approached the bottom of the ponds. During the field campaign clear differences in snow cover thickness of about 20 to 30 cm were observed between the ponds. At all investigated ponds, a layer of depth hoar was observed to form the base of the snow cover. In contrast, almost no snow accumulation was found at the larger lakes.

4.2 Distribution of gas bubbles within the ice cover

Most of the ice columns were very clear with only a few visible bubbles. After a short warm event during the field campaign a very thin layer of white ice (1–3 cm) was observed above black ice at some locations. This white ice layer was excluded from further analysis. The ice columns from the ISP1 and ISP2 ponds showed a layer of abundant bubbles close to the bottom of the ponds, starting from a depth of about 15 cm. Moss stems in the sediments on the floor of these two ponds were usually completely surrounded by bubbles. The diameter of these bubbles ranged from about 1 mm to 5 mm. Two or three thin layers of bubbles were also observed in these two ponds at depths of between 5 and 15 cm. Three very thin layers of bubbles were also observed at similar depths (between 5 and 15 cm) in the ice columns from pond ISP3. The consistent occurrence of these thin bubble layers in similar depths and different ponds indicates a formation related to air pressure changes. However, the sizes of these bubbles layers were assessed to be negligible compared to the ice sample sizes. The ice columns from the relatively deep ponds (ASP1, ASP2, and ASP3), which had depths greater than 0.5 m, did not reach the bottom and hence the presence or absence of a layer of abundant bubbles close to the bottom of the ponds (as seen in the shallow ISP1 and ISP2 ponds) could not be verified. The ice columns from pond ASP3 revealed a narrow bubble layer at about 15 cm depth similar to that seen in the shallow ponds, but those from ponds ASP1 and ASP2 showed no visible bubbles between the surface and a depth of 35 cm. However, all ice columns from the deep ponds were consistent in showing two to three thin bubble layers between depths of 35 and 40 cm.

BGD
11, 11061–11094, 2014

4.3 Methane concentrations in lake and pond ice

The CH_4 concentrations obtained from all ice samples are show in Figure 5, where they are plotted semi-logarithmically against the ratio of sample depth to maximum water depth. The whiskers following the orientation of the depth axis indicate the sample size while the whiskers following the orientation of the concentration axis indicate uncertainties in the measured CH_4 concentrations according to the Monte-Carlo simulations (see Sect. 3.3). In addition, the samples are color coded according to the surface area of the lake or pond from which they were obtained. The CH_4 concentration within the ice cover showed considerable variation, ranging from the detection limit of the gas analyzer up to 0.08 mol m^{-3}. The detection limit of the used GC setup was at about 1 ppm which would equate to a detection limit of about 5×10^{-5} mol m^{-3} considering sample size and head space volume. On average about 2×10^{-3} mol m^{-3} (0.03 g_{CH_4} m^{-3}) was stored in the ice cover between the surface and a depth of 0.65 m. However, these concentrations varied over two orders of magnitude indicating marked differences between the different waterbody types. The CH_4 concentration was generally observed to increase with depth. The highest CH_4 concentrations were recorded from waterbodies with surface areas of less than 50 m^2 and in ice samples from close to the bottom of waterbodies. The results suggest an exponential relationship between CH_4 concentration and ice cover thickness; the measured concentrations generally followed an exponential trend, with the exception of four outliers. A detailed analysis of individual CH_4 profiles confirmed the exponential increase in CH_4 concentrations with depth and the marked differences between waterbodies (see Fig. 6). An exponential increase in CH_4 concentration was recorded for all ponds in which the acquired ice columns reached close to the bottom of the waterbody. The lowest CH_4 concentrations were recorded in the ice columns from large thermokarst lakes. In these lakes only the uppermost part of the ice cover was sampled relative to the maximum lake depths. However, four outliers occurred with high concentrations of up to 0.08 mol m^{-3}. Three of four outliers were observed at thermokarst lakes with surface areas larger than 10^4 m^2.

BGD
11, 11061–11094, 2014

4.4 Modeling methane storage in the ice cover

The CH_4 profiles from the ISP1, ISP2, and ISP3 ponds were from ponds with maximum depths of less than 0.5 m. The morphology of these ponds still placed them within the ISP category, despite some early signs of degradation. In contrast, the ASP1, ASP2, and ASP3 ponds had maximum depths greater than 0.5 m (up to 1.2 m) and fell into the ASP category.

The maximum CH_4 concentrations measured in the ISP1, ISP3, and ASP3 samples were about one order of magnitude higher than those from the other profiles. The ice samples were typically 5 to 10 cm high which placed a limit on the depth resolution, but this was improved to some extent by overlap between samples. The uncertainty in the CH_4 concentration from each sample was relatively low although some differences were observed between overlapping samples, especially in those from the ASP1 and ASP2 ponds. Despite these uncertainties and the limited depth resolution all ponds consistently revealed an exponential increase in CH_4 concentration with depth (Fig. 6). The ASP3 profile in particular showed a very sharp increase in concentration in the deepest sample. The increase in CH_4 concentrations in the ISP1 and ISP2 coincided with increased bubble densities, but no general relationship was observed between bubble density and CH_4 concentration in the ISP3, ASP1, ASP2, and ASP3 ponds.

The derived CH_4 concentration profiles for six of the ponds were analyzed and the mass balance model fitted to these profiles in order to estimate net CH_4 production rates (see Sect. 3.4). From this fitting procedure the effective bubble cross-sections and net CH_4 production rates were obtained for all the analyzed ponds, and also for an additional ASP (ASP4). The model was able to reproduce the observed CH_4 concentration profiles for all of the ponds. The best fit results and the 95 % confidence intervals of the fitting procedure are shown in Fig. 6. Most of the differences between the best fit and the actual measurements fall within the 95 % confidence interval of the model output, taking into account the depth resolution and the uncertainties in the measured CH_4 concentrations. The model also successfully reproduced the sharp increase in

BGD
11, 11061–11094, 2014

CH_4 concentration noted in the ASP3 profile. In this particular case the model simulated the storage of excess CH_4 in the ice cover, since the maximum solubility of CH_4 in water (about 2.5 mol m^{-3} at about 0 °C and 1000 hPa) was reached in the shrinking water column.

The inferred net CH_4 production rates resulting from the fitting procedure revealed marked variations in net CH_4 production between the different waterbodies (Fig. 7). The net production rates ranged from 10^{-11} to 10^{-7} mol m^{-2} s^{-1} (0.01 to 140 mg_{CH_4} m^{-2} d^{-1}) and the effective bubble cross-sections ranged from 10^{-4} m to 10^{-2} m. The net CH_4 production rate was generally higher in profiles with smaller effective bubble cross-sections. The highest net CH_4 production rates were calculated for the ASP1, ASP2, ASP3, and ASP4 which had maximum water depths greater than 0.5 m and showed clear signs of recent permafrost degradation. In contrast, lower net CH_4 production rates but larger bubble cross-sections were calculated for the ISP1, ISP2, and ISP3.

5 Discussion

5.1 Characteristics and sensitivities of Arctic ponds

The survey of ponds and lakes within the study area clearly showed an abundance of ponds in the lowland tundra landscape of the Lena River Delta. Almost 10 % of the total land surface was occupied by waterbodies with surface areas of less than 300 m^2, most of which were no deeper than 1 m. The abundance of small waterbodies in the Arctic has been noted in a number of previous studies (Emmerton et al., 2007; Grosse et al., 2008). However, a recent study by Muster et al. (2012) suggested that the number of small waterbodies in permafrost regions may have been considerably underestimated. In the study area, and also in many other permafrost regions, the current climatic conditions allow these small, shallow ponds to freeze completely during winter and permafrost is therefore preserved under most of these small ponds. How-

BGD
11, 11061–11094, 2014

ever, this study has demonstrated that the freezing rates of ponds can vary greatly from one pond to another, and from one year to another. Ice thicknesses measurements from two consecutive years revealed a difference in ice cover thickness of about 40 %. Detailed investigations of the surface energy balance within the study area have suggested that marked interannual differences in the freezing rate can be largely attributed to differences in the snow cover and the wintertime cloud cover (Langer et al., 2011b). This means that small ponds and the underlying permafrost are likely to be highly sensitive to any changes in wintertime synoptic conditions that may occur as a result of predicted climatic warming in the Arctic (e.g. Hinzman et al., 2005). A reduction in the freezing rate would prolong the period during which unfrozen sediments are available to microbial decomposition. In addition, a sustained reduction in freezing depth would lead to the formation of continuously unfrozen sediments (talik) beneath the deeper ponds. The formation of talik can facilitate increased shoreline erosion and lake growth, resulting in further deepening of the unfrozen sediment layer. These small waterbodies therefore have the potential to trigger major changes in Arctic landscapes and ecosystems. The survey of waterbodies also revealed that a large fraction of ponds are no deeper than 20 cm. These shallow ponds occur mainly in low-centered polygons with little or no signs of degradation. The occurrence and size of such ponds is assumed to be directly related to the polygonal micro-topography, which also explains why no relationship could be observed between pond size and water depth. There is a clear contrast with the frequency of ponds deeper than 0.5 m. These ponds show a more uniform depth distribution with a slight maximum between 0.5 and 1 m. A clear depth–size relationship was observed for these deeper ponds. The existence of such a relationship suggests a link between the erosive processes leading to the deepening of the pond and the size of the waterbody. However, the poorly defined depth–size relationships indicates a rather complex interrelationship.

BGD
11, 11061–11094, 2014

5.2 CH_4 concentrations and net production rates

All of the CH_4 profiles derived from ice samples indicate an exponential increase in CH_4 concentration with depth, which is in agreement with previous observations by Phelps et al. (1998) from various Alaskan and Canadian lakes. The consistency between these two studies suggests that both freeze-degassing of CH_4 and CH_4 storage within the ice cover generally involve the same processes. Some individual concentrations have been observed to deviate from the general exponential behavior. These outliers may be explained by the admixture of ebullition bubbles, which are not explicitly accounted for in this study. However, the exponential relationship between ice depth and CH_4 concentration can be reproduced by a simplified mass balance model, assuming constant net CH_4 production and bubble accumulation. The exponential shape results from the dynamic balance between net CH_4 production, freeze-degassing, and storage of CH_4 within the ice cover. The mass balance model was successfully fitted to the measured CH_4 concentrations by optimizing the net CH_4 production rate and the effective bubble size. A high level of confidence was achieved in all profiles. Furthermore, the model was able to realistically reproduce the sharp increase in CH_4 concentration observed in one of the profiles. This indicated that the model was able to accurately represent the timing of CH_4 saturation in the shrinking water column during freezing. The overall high level of performance of the model for the different profiles suggests that the basic process of CH_4 freeze-degassing and storage in the ice cover is adequately represented. In addition, sensitivity tests revealed that the fit was very robust against variations in the initial values of net CH_4 production and effective bubble size. This inspires confidence that the magnitudes of the fitted net CH_4 production and bubble accumulation rates are realistic. The results were also found to be robust against uncertainties in the initial CH_4 concentration within the water column, prior to the onset of freezing. Nevertheless, unpredictable errors due to gas loss from the edges of the samples or methane oxidation within the ice could negatively bias the measured concentration rates, and consequently the resulting net CH_4 production rates. Oversimplified model

BGD
11, 11061–11094, 2014

assumptions, such as uniformly distributed CH_4 concentrations and a constant rate of bubble accumulation, could also affect the net CH_4 production rates. The model results must therefore be considered to represent first order estimates. The results of the fitting procedure generally suggest marked differences in the net CH_4 production from different pond types. Initial state ponds (water depth < 0.5 m) show very low net production rates, of the order of 10^{-11} and 10^{-10} mol m^{-2} s^{-1} (0.01 to 0.14 mg_{CH_4} m^{-2} d^{-1}). In contrast, advanced state ponds (depth > 0.5 m) with clear signs of thermal erosion show net CH_4 production rates of the order of 10^{-7} mol m^{-2} s^{-1} (140 mg_{CH_4} m^{-2} d^{-1}). Similar ranges of CH_4 emission rates have previously been reported in summer from ponds in a similar type of landscape on Bylot Island, Canada (Laurion et al., 2010). The net CH_4 production rates from the ponds at our study area were of a similar magnitude to observed summertime CH_4 emission rates (excluding ebullition) from ice-wedge ponds on Bylot Island. The ice-wedge ponds on Bylot Island mainly occur within collapsed polygonal structures and could by classified as ASPs (Negandhi et al., 2013). Significantly lower CH_4 emission rates were reported from intra-polygonal ponds on Bylot Island, which may correspond to our ISP class. These results provide further evidence that the marked differences in net CH_4 production rates between the different pond types are likely to be due to fundamental differences in biogeochemical processes resulting from active thermal erosion (Laurion et al., 2010; Rautio et al., 2011; Laurion and Mladenov, 2013). The differences in net CH_4 production may also be related to differences in the vegetation growing on the floor of the ponds. The vegetation in ISPs within the study area often consists of the brown mosses *Scorpidium scorpioides* (Liebner et al., 2011). These mosses live in symbiosis with metamorphic CH_4-oxidizing bacteria that could effectively limit CH_4 emission (Liebner et al., 2011). Photosynthesis and oxygen production are still possible beneath the growing ice cover during early winter. Indicators of active photosynthesis in ISPs during freezing is provided by the large number of bubbles observed around moss stems (see Sect. 4.2). However, other processes such as CO_2 emission through moss respiration or preferential bubble nucleation at the moss stems could have contribute to the formation of these bubble clusters.

BGD
11, 11061–11094, 2014

The maximum summertime CH_4 emission rates from the average tundra landscape on Samoylov Island are of the order of 5×10^{-8} mol m^{-2} s^{-1} (60 mg_{CH_4} m^{-2} d^{-1}) (Sachs et al., 2008; Wille et al., 2008). This is half an order of magnitude less than the winter net CH_4 production rates from ASPs, stressing the importance of ponds and the freezing period to the local carbon cycle. Even small waterbodies must therefore be considered hotspots of CH_4 production in a tundra landscape. It is, however, important to note that our results do not take into account CH_4 that is transported and stored in the ice cover through ebullition, and the total CH_4 production from ASPs is therefore likely to be much greater than our modeling suggests.

6 Conclusions

Our results show that ponds in the polygonal tundra can be important sources of CH_4 during the freezing period. Extensive measurements in the ice cover of different ponds have revealed that the CH_4 concentrations increase exponentially with depth, indicating intensive CH_4 production under the growing ice cover. Inverse modeling has revealed high net CH_4 production rates in ponds showing signs of erosion in the surrounding permafrost, which contrasts with the low net production rates observed in ponds with almost intact permafrost. These results have far ranging implications for the CH_4 emission potential of lowland tundra landscapes, since:

- The CH_4 that is produced during the freezing period is likely to be released into the atmosphere during the spring melt. Ponds therefore make a significant contribution to the greenhouse gas emission budget of the tundra.
- Ponds are abundant in lowland tundra landscapes and their formation is closely related to the thermal state and stability of the permafrost. Hence, the degradation of permafrost may affect the CH_4 emissions from tundra landscapes.
- The net production of CH_4 from ponds that show signs of thermal erosion in the surrounding permafrost is observed to be two to three orders of magnitude greater

BGD
11, 11061–11094, 2014

than from ponds located within largely intact permafrost. Any future warming-induced erosion and pond expansion may therefore greatly increase the CH_4 emission potential of tundra landscapes.

– The freezing rate of ponds is highly sensitive to the winter synoptic conditions. Any future changes in winter conditions associated with a warming climate may further prolong the time available for CH_4 production in ponds.

Appendix:

The mass balance of methane in a freezing pond can be written as

$$N_i + N_g + N_a - N_0 - N_P = 0, \quad (1)$$

where N_i is the amount of CH_4 molecules that are stored in the ice cover, N_g is the amount of methane stored in bubbles at the ice–water interface, N_a is the number of dissolved methane molecules in the water column, N_0 is the amount of dissolved methane that is stored in the water column at the start of freezing, and N_P is the number of CH_4 molecules produced. The individual CH_4 components of the mass balance are parameterized as

$$N_i = A_b \int_0^t C(\tau) \frac{\partial z(\tau)}{\partial \tau} d\tau, \quad (2)$$

$$N_g = C(t) V_b, \quad (3)$$

$$N_a = C(t) k_H R T_w (z_0 - z(t)), \quad (4)$$

$$N_0 = C_0 z_0, \quad (5)$$

$$N_P = \int_0^t P(\tau) d\tau, \quad (6)$$

BGD
11, 11061–11094, 2014

where $C(t)$ is the concentration of methane in bubbles at the ice–water interface at time t; k_H is the Henry's law constant of methane, assuming constant pressure and a water temperature T_w of 273.15 K; R is the universal gas constant; A_b is the effective bubble size in direct contact with the ice–water interface; $z(t)$ is the ice cover thickness; V_b is the effective volume of bubbles at the ice–water interface; z_0 is the depth of the water column at the start of freezing; C_0 is the concentration of methane in water at the start of freezing; and P is the rate of net methane production in the pond. Equation (4) is modified to

$$N_a = k_H(z_0 - z(t)), \tag{7}$$

as soon as CH_4 saturation is reached in the remaining water column so that all excess methane is deposited directly into the ice cover. Thus, combining the Eqs. (1)–(7) results in two first order linear differential equations for (i) the duration of CH_4 undersaturation ($t \le t_S$) and (ii) the period of CH_4 saturation ($t > t_S$)

$$\begin{aligned} aC(t) + b\frac{\partial C(t)}{\partial t} - P(t) = 0, \qquad & \text{for } 0 \le t \le t_S \\ cC(t) + d\frac{\partial C(t)}{\partial t} - e - P(t) = 0, \qquad & \text{for } t > t_S \end{aligned}, \tag{8}$$

where a, b, c, d, and e summarize the parameters according to Eqs. (2)–(7). The differential equations can be solved with exponential functions so that the concentration of methane in the water column and in the ice cover can be calculated for each time step in the freezing process.

Acknowledgements. Special thanks go to Katrin Fröb and Karoline Morling for their invaluable work in the field and laboratory. Furthermore, we thank Waldemar Schneider and our Russian partners at AARI and the Lena Delta Reserve for the logistical support of our field work. We gratefully acknowledge the financial support by the Helmholtz Association through a grant (VH-NG 203) awarded to Julia Boike. Furthermore, the authors acknowledge the financial support by the European Union FP7-ENV project PAGE21 under contract number GA282700.

BGD
11, 11061–11094, 2014

References

Abnizova, A., Siemens, J., Langer, M., and Boike, J.: Hydrochemistry, water level, and discharge of water from Samoylov Island, Lena Delta, northeastern Siberia, in 2008, Supplement, Global Biogeochem. Cy., 26, GB2041, doi:10.1029/2011GB004237, 2012a. 11071

Abnizova, A., Siemens, J., Langer, M., and Boike, J.: Small ponds with major impact: the relevance of ponds and lakes in permafrost landscapes to carbon dioxide emissions, Global Biogeochem. Cy., 26, 1–9, 2012b. 11063

Anderson, G.: Error propagation by the Monte Carlo method in geochemical calculations, Geochim. Cosmochim. Ac., 40, 1533–1538, 1976. 11069

Boereboom, T., Depoorter, M., Coppens, S., and Tison, J.-L.: Gas properties of winter lake ice in Northern Sweden: implication for carbon gas release, Biogeosciences, 9, 827–838, doi:10.5194/bg-9-827-2012, 2012. 11063, 11064, 11069

Boike, J., Langer, M., Lantuit, H., Muster, S., Roth, K., Sachs, T., Overduin, P., Westermann, S., and McGuire, A.: Permafrost – physical aspects, carbon cycling, databases and uncertainties, in: Recarbonization of the Biosphere, edited by: Lal, R., Lorenz, K., Hüttl, R. F., Schneider, B. U., and von Braun, J., Springer, Netherlands, 159–185, 2012. 11063

Boike, J., Kattenstroth, B., Abramova, K., Bornemann, N., Chetverova, A., Fedorova, I., Fröb, K., Grigoriev, M., Grüber, M., Kutzbach, L., Langer, M., Minke, M., Muster, S., Piel, K., Pfeiffer, E.-M., Stoof, G., Westermann, S., Wischnewski, K., Wille, C., and Hubberten, H.-W.: Baseline characteristics of climate, permafrost and land cover from a new permafrost observatory in the Lena River Delta, Siberia (1998–2011), Biogeosciences, 10, 2105–2128, 2013, http://www.biogeosciences.net/10/2105/2013/. 11065

Brosius, L., Walter Anthony, K., Grosse, G., Chanton, J., Farquharson, L., Overduin, P. P., and Meyer, H.: Using the deuterium isotope composition of permafrost meltwater to constrain thermokarst lake contributions to atmospheric CH_4 during the last deglaciation, J. Geophys. Res.-Biogeo., 117, G01022, doi:10.1029/2011JG001810, 2012. 11063

Brown, J., Ferrians Jr, O., Heginbottom, J., and Melnikov, E.: Circum-Arctic Map of Permafrost and Ground-Ice Conditions, US Geological Survey Circum-Pacific Map, 1997. 11088

Carte, A.: Air bubbles in ice, P. Phys. Soc., 77, 757–768, 1961. 11064, 11070

Cole, J. J., Prairie, Y. T., Caraco, N. F., McDowell, W. H., Tranvik, L. J., Striegl, R. G., Duarte, C. M., Kortelainen, P., Downing, J. A., Middelburg, J. J., and Melack, J.: Plumbing the global

BGD
11, 11061–11094, 2014

carbon cycle: integrating inland waters into the terrestrial carbon budget, Ecosystems, 10, 172–185, 2007. 11063
Craig, H., Wharton, R., and McKay, C.: Oxygen supersaturation in ice-covered Antarctic lakes: biological versus physical contributions, Science, 255, 318–321, 1992. 11064
Emmerton, C. A., Lesack, L. F., and Marsh, P.: Lake abundance, potential water storage, and habitat distribution in the Mackenzie River Delta, western Canadian Arctic, Water Resour. Res., 43, W05419, doi:10.1029/2006WR005139, 2007. 11063, 11076
Grigoriev, N.: The temperature of permafrost in the Lena delta basin – deposit conditions and properties of the permafrost in Yakutia, 97–101, 1960 (in Russian). 11065
Grosse, G., Romanovsky, V., Walter, K., Morgenstern, A., Lantuit, H., and Zimov, S.: Distribution of thermokarst lakes and ponds at three yedoma sites in Siberia, in: Proceedings of the 9th International Conference on Permafrost, Fairbanks, Alaska, 29 June–3 July 2008, 551–556, 2008. 11063, 11076
Helbig, M., Boike, J., Langer, M., Schreiber, P., Runkle, B. R., and Kutzbach, L.: Spatial and seasonal variability of polygonal tundra water balance: Lena River Delta, northern Siberia (Russia), Hydrogeol. J., 21, 133–147, 2013. 11066
Hinzman, L., Bettez, N., Bolton, W., Chapin, F., Dyurgerov, M., Fastie, C., Griffith, B., Hollister, R., Hope, A., Huntington, H., Jensen, A., Jia, G., Jorgenson, T., Kane, D., Klein, D., Kofinas, G., Lynch, A., Lloyd, A., McGuire, A., Nelson, F., Oechel, W., Osterkamp, T., Racine, C., Romanovsky, V., Stone, R., Stow, D., Sturm, M., Tweedie, C., Vourlitis, G., Walker, M., Walker, D., Webber, P., Welker, J., Winker, K., and Yoshikawa, K.: Evidence and implications of recent climate change in Northern Alaska and other Arctic regions, Climatic Change, 72, 251–298, 2005. 11077
Hugelius, G., Tarnocai, C., Broll, G., Canadell, J. G., Kuhry, P., and Swanson, D. K.: The Northern Circumpolar Soil Carbon Database: spatially distributed datasets of soil coverage and soil carbon storage in the northern permafrost regions, Earth Syst. Sci. Data, 5, 3–13, doi:10.5194/essd-5-3-2013, 2013. 11063
Karlsson, J., Giesler, R., Persson, J., and Lundin, E.: High emission of carbon dioxide and methane during ice thaw in high latitude lakes, Geophys. Res. Lett., 40, 1123–1127, 2013. 11063
Killawee, J., Fairchild, I., Tison, J.-L., Janssens, L., and Lorrain, R.: Segregation of solutes and gases in experimental freezing of dilute solutions: implications for natural glacial systems, Geochim. Cosmochim. Ac., 62, 3637–3655, 1998. 11064

BGD
11, 11061–11094, 2014

Koven, C. D., Ringeval, B., Friedlingstein, P., Ciais, P., Cadule, P., Khvorostyanov, D., Krinner, G., and Tarnocai, C.: Permafrost carbon–climate feedbacks accelerate global warming, P. Natl. Acad. Sci. USA, 108, 14769–14774, 2011. 11063

Kutzbach, L., Wille, C., and Pfeiffer, E.-M.: The exchange of carbon dioxide between wet arctic tundra and the atmosphere at the Lena River Delta, Northern Siberia, Biogeosciences, 4, 869–890, doi:10.5194/bg-4-869-2007, 2007. 11066

Lachenbruch, A. H.: Mechanics of thermal contraction cracks and ice-wedge polygons in permafrost, Geol. S. Am. S., 70, 1–66, 1962. 11066

Langer, M., Westermann, S., Muster, S., Piel, K., and Boike, J.: The surface energy balance of a polygonal tundra site in northern Siberia – Part 1: Spring to fall, The Cryosphere, 5, 151–171, doi:10.5194/tc-5-151-2011, 2011a. 11065

Langer, M., Westermann, S., Muster, S., Piel, K., and Boike, J.: The surface energy balance of a polygonal tundra site in northern Siberia – Part 2: Winter, The Cryosphere, 5, 509–524, doi:10.5194/tc-5-509-2011, 2011b. 11077

Laurion, I. and Mladenov, N.: Dissolved organic matter photolysis in Canadian arctic thaw ponds, Environ. Res. Lett., 8, 35026–35037, 2013. 11079

Laurion, I., Vincent, W. F., MacIntyre, S., Retamal, L., Dupont, C., Francus, P., and Pienitz, R.: Variability in greenhouse gas emissions from permafrost thaw ponds, Limnol. Oceanogr., 55, 115–133, 2010. 11063, 11079

Liebner, S., Zeyer, J., Wagner, D., Schubert, C., Pfeiffer, E.-M., and Knoblauch, C.: Methane oxidation associated with submerged brown mosses reduces methane emissions from Siberian polygonal tundra, J. Ecol., 99, 914–922, 2011. 11079

Lipp, G., Körber, C., Englich, S., Hartmann, U., and Rau, G.: Investigation of the behavior of dissolved gases during freezing, Cryobiology, 24, 489–503, 1987. 11064

McGuire, A. D., Anderson, L. G., Christensen, T. R., Dallimore, S., Guo, L., Hayes, D. J., Heimann, M., Lorenson, T. D., Macdonald, R. W., and Roulet, N.: Sensitivity of the carbon cycle in the Arctic to climate change, Ecol. Monogr., 79, 523–555, 2009. 11063

Morgenstern, A., Ulrich, M., Günther, F., Roessler, S., Fedorova, I. V., Rudaya, N. A., Wetterich, S., Boike, J., and Schirrmeister, L.: Evolution of thermokarst in East Siberian ice-rich permafrost: a case study, Geomorphology, 201, 363–379, 2013. 11066

Muster, S., Langer, M., Heim, B., Westermann, S., and Boike, J.: Subpixel heterogeneity of ice-wedge polygonal tundra: a multi-scale analysis of land cover and evapotranspiration in the Lena River Delta, Siberia, Tellus B, 64, 1–19, 2012. 11063, 11066, 11067, 11076

BGD
11, 11061–11094, 2014

Muster, S., Heim, B., Abnizova, A., and Boike, J.: Water body distributions across scales: a remote sensing based comparison of three arctic tundra wetlands, Remote Sens., 5, 1498–1523, 2013. 11063

Negandhi, K., Laurion, I., Whiticar, M. J., Galand, P. E., Xu, X., and Lovejoy, C.: Small thaw ponds: an unaccounted source of methane in the Canadian High Arctic, PLOS ONE, 8, e78204, doi:10.1371/journal.pone.0078204, 2013. 11066, 11079

O'Connor, F. M., Boucher, O., Gedney, N., Jones, C. D., Folberth, G. A., Coppell, R., Friedlingstein, P., Collins, W. J., Chappellaz, J., Ridley, J., and Johnson, C. E.: Possible role of wetlands, permafrost, and methane hydrates in the methane cycle under future climate change: a review, Rev. Geophys., 48, RG4005, doi:10.1029/2010RG000326, 2010. 11063

Phelps, A. R., Peterson, K. M., and Jeffries, M. O.: Methane efflux from high-latitude lakes during spring ice melt, J. Geophys. Res.-Atmos., 103, 29029–29036, 1998. 11065, 11078

Rautio, M., Dufresne, F., Laurion, I., Bonilla, S., Vincent, W. F., and Christoffersen, K. S.: Shallow freshwater ecosystems of the circumpolar Arctic, Ecoscience, 18, 204–222, 2011. 11079

Sachs, T., Wille, C., Boike, J., and Kutzbach, L.: Environmental controls on ecosystem-scale CH_4 emission from polygonal tundra in the Lena River Delta, Siberia, J. Geophys. Res.-Biogeo., 113, G00A03, doi:10.1029/2007JG000505, 2008. 11080

Walter, K., Zimov, S., Chanton, J., Verbyla, D., and Chapin, F.: Methane bubbling from Siberian thaw lakes as a positive feedback to climate warming, Nature, 443, 71–75, 2006. 11063

Walter Anthony, K. M. and Anthony, P.: Constraining spatial variability of methane ebullition seeps in thermokarst lakes using point process models, J. Geophys. Res.-Biogeo., 118, 1015–1034, 2013. 11063, 11064, 11070

Walter Anthony, K. M., Vas, D. A., Brosius, L., Chapin III, F. S., Zimov, S. A., and Zhuang, Q.: Estimating methane emissions from northern lakes using ice-bubble surveys, Limnol. Oceanogr.-Meth., 8, 592–609, 2010. 11063, 11064

Wei, P., Huang, C., and Lee, K.: Nucleation of bubbles on a solidification front – experiment and analysis, Metall. Mater. Trans. B, 34, 321–332, 2003. 11064

Wetterich, S., Schirrmeister, L., Meyer, H., Viehberg, F. A., and Mackensen, A.: Arctic freshwater ostracods from modern periglacial environments in the Lena River Delta (Siberian Arctic, Russia): geochemical applications for palaeoenvironmental reconstructions, J. Paleolimnol., 39, 427–449, 2008. 11066

BGD
11, 11061–11094, 2014

Wik, M., Crill, P. M., Bastviken, D., Danielsson, Å., and Norbäck, E.: Bubbles trapped in arctic lake ice: potential implications for methane emissions, J. Geophys. Res.-Biogeo., 116, G03044, doi:10.1029/2011JG001761, 2011. 11063, 11064

Wille, C., Kutzbach, L., Sachs, T., Wagner, D., and Peiffer, E.: Methane emission from Siberian arctic polygonal tundra: eddy covariance measurements and modeling, Glob. Change Biol., 14, 1395–1408, 2008. 11080

Yoshimura, K., Inada, T., and Koyama, S.: Growth of spherical and cylindrical oxygen bubbles at an ice–water interface, Cryst. Growth Des., 8, 2108–2115, 2008. 11064, 11065, 11070

Zimov, S., Voropaev, Y. V., Semiletov, I., Davidov, S., Prosiannikov, S., Chapin, F. S., Chapin, M., Trumbore, S., and Tyler, S.: North Siberian lakes: a methane source fueled by Pleistocene carbon, Science, 277, 800–802, 1997. 11063

BGD
11, 11061–11094, 2014

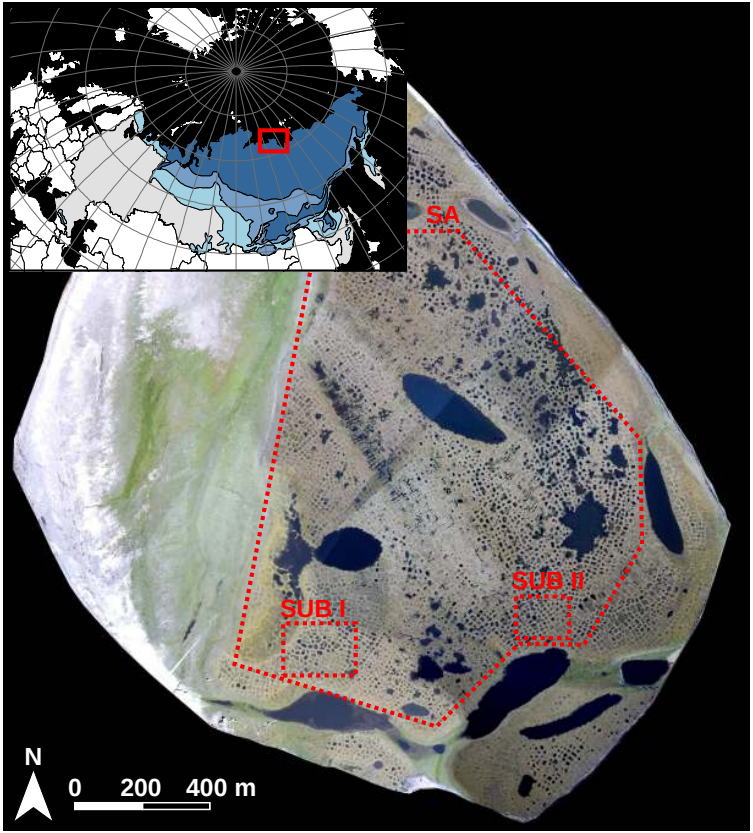

Figure 1. Location of the study area in northern Siberia within the zone of continuous permafrost **(a)** (map after: Brown et al., 1997), and ortho-rectified aerial image of Samoylov Island **(b)**. The main study area (SA) and the two sub-areas (SUB I, SUB II) used for the pond and lake mapping and for sampling are outlined in red.

BGD
11, 11061–11094, 2014

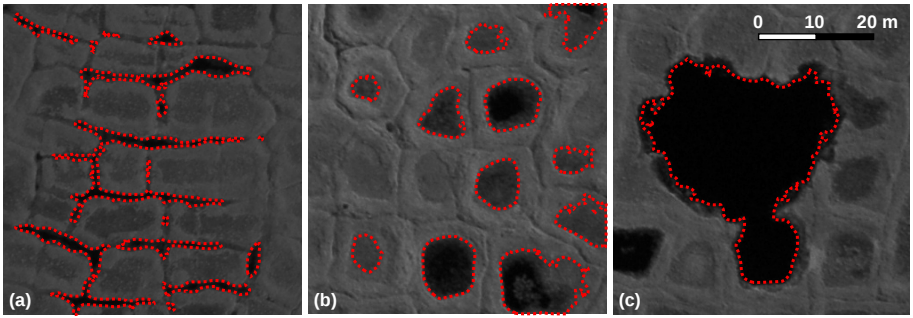

Figure 2. Typical ponds in the polygonal tundra mapped from near infrared (NIR) areal images. Initial state ponds (ISPs) include **(a)** ice-wedge ponds and **(b)** intra-polygonal ponds within intact polygonal structures. Advanced state ponds (ASPs) show clear signs of degradation of the polygonal structures and include merged intra-polygonal ponds **(c)**, expanded ice-wedge ponds, and combinations of both.

BGD
11, 11061–11094, 2014

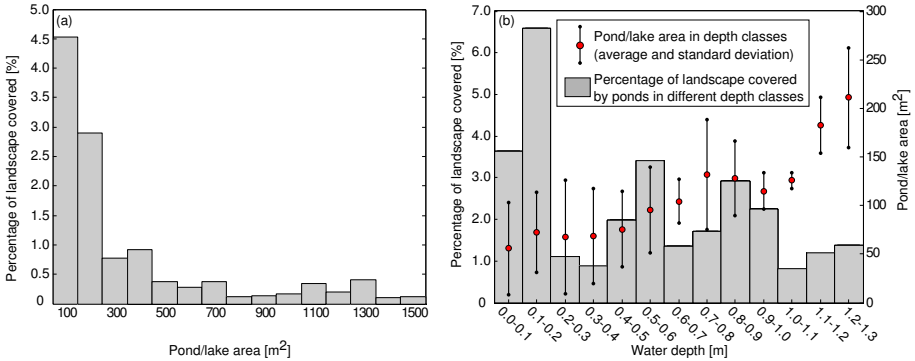

Figure 3. Percentage of landscape covered by ponds in different size classes (waterbodies larger 1500 m^2 are excluded) **(a)**. Percentage of landscape covered by ponds in different depth classes **(b)**. The secondary y-axis in **(b)** shows the average surface area for each depth class. The whiskers indicate the standard deviation for each depth class.

BGD
11, 11061–11094, 2014

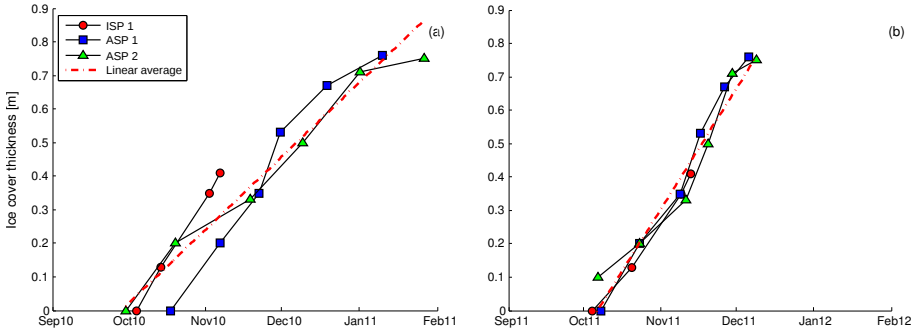

Figure 4. Growth of ice cover inferred from water temperature measurements in three different ponds during **(a)** the winter of 2010–2011, and **(b)** the winter of 2011–2012.

BGD
11, 11061–11094, 2014

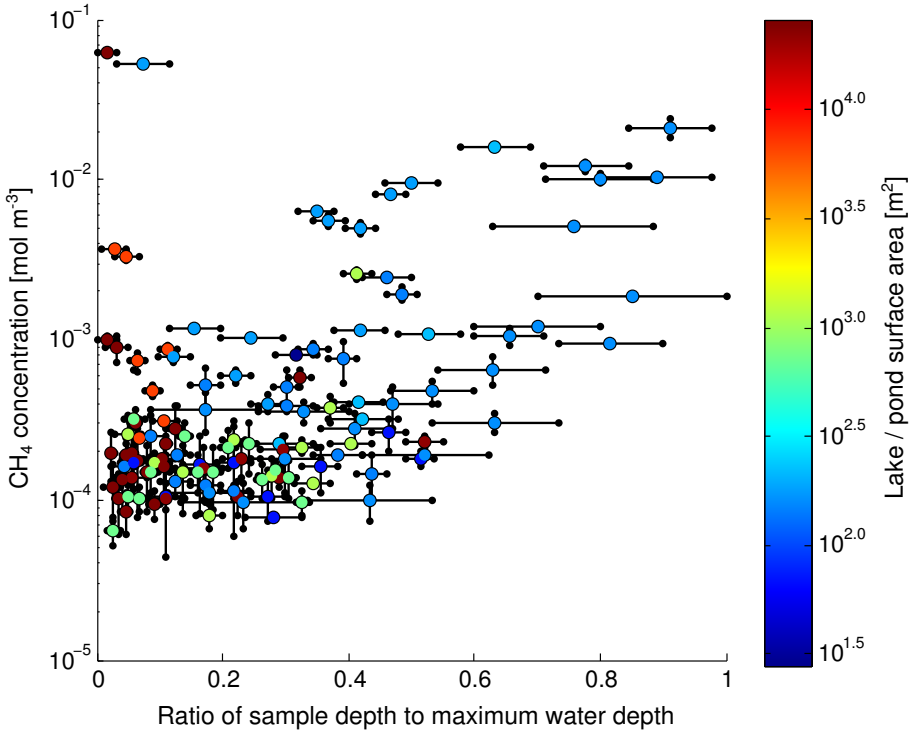

Figure 5. Methane concentrations within the ice cover of different lakes and ponds, plotted against the ratio of sample depth to maximum water depth (note the logarithmic scale). The circles representing individual samples are colored according to the surface area of the lake or pond from which they came.

BGD
11, 11061–11094, 2014

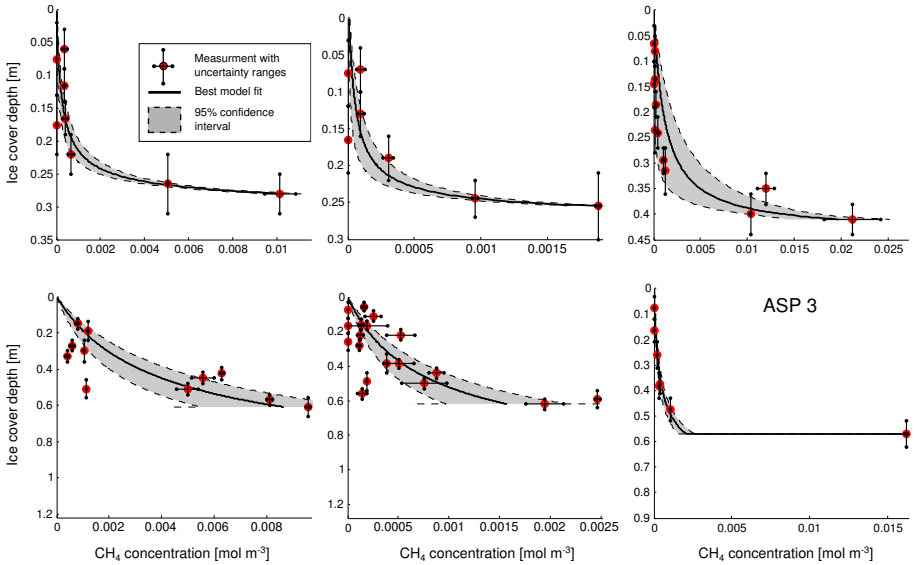

Figure 6. Measured and modeled CH_4 concentrations in the ice cover of different ponds. The whiskers show the measurement uncertainty of the model and the shaded areas indicate the 95 % confidence interval.

BGD
11, 11061–11094, 2014

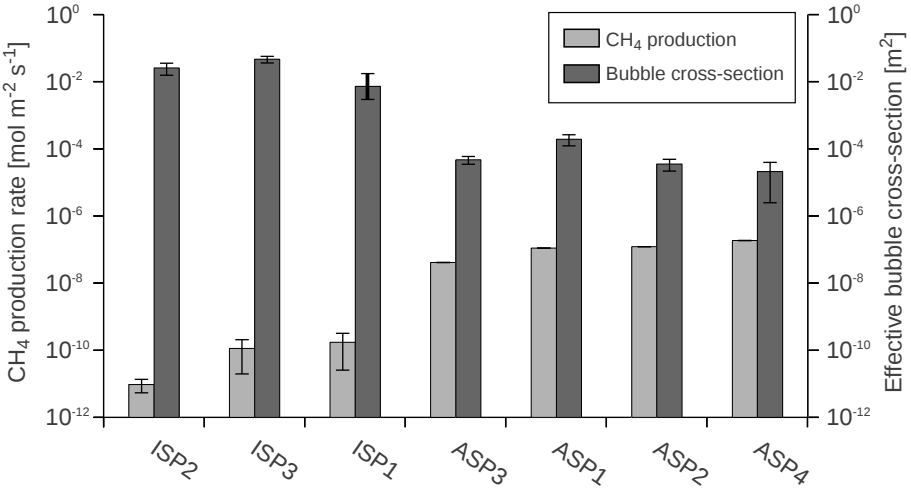

Figure 7. Net methane production and effective bubble cross-section for different ponds, calculated by inverse modeling using the 1-D mass balance model (note the logarithmic scale). The whiskers indicate the 95 % confidence interval of the model results.

BGD
11, 11061–11094, 2014